

A&A manuscript no.

(will be inserted by hand later)

Your thesaurus codes are:

03 (11.09.1 NGC 7331; 11.09.4; 11.19.2; 11.19.6; 13.19.1, 09.13.2)

ASTRONOMY
AND
ASTROPHYSICS

Molecular gas in the bulge and ring of NGC 7331

F.P. Israel¹ and F. Baas^{1,2}¹ Sterrewacht Leiden, P.O. Box 9513, NL 2300 RA Leiden, The Netherlands² Joint Astronomy Centre, 660 N. A'ohoku Pl., Hilo, Hawaii, 96720, USA

Received 6 January 1999; accepted 5 August 1999

Abstract. CO emission from the Sb(rs)I-II galaxy NGC 7331 has been mapped in the $J=2-1$ transition with a $21''$ beam over an area $3.5'$ by $1.3'$. A relatively low contrast enhancement of molecular line emission occurs in a ring-like zone at a distance of approximately 3.5 kpc from the center; there is no evidence for a pronounced central hole. The ring is located at the edge of the region of rigid rotation and roughly coincides with an inhomogeneous ring of nonthermal radio continuum emission. It is well inside the radius of maximum rotational velocity.

The intensities of the 492 GHz [CI] line and various ^{12}CO and ^{13}CO transitions observed towards the center and two outlying positions are modelled by multiple molecular gas components: low-density gas at a kinetic temperature $T_{\text{kin}} \approx 10$ K, and high-density gas at both $T_{\text{kin}} \approx 10$ K and $T_{\text{kin}} \approx 20$ K. The molecular gas must be distributed in clumpy or filamentary form. The CO-to- H_2 conversion factor X applicable to the bulge is only half that applicable to the ring and beyond. The latter is still significantly lower than X_{MilkyWay} . Molecular hydrogen is the dominant mass contributor to the interstellar medium in the bulge and in the ring. Far-infrared emission from dust peaks inside the ring at $100\mu\text{m}$ (warm dust), and in the ring at $850\mu\text{m}$ (colder dust). Beyond the ring, neutral atomic hydrogen is dominant. Inferred total hydrogen mass densities in the ring are about twice those in the bulge. Interstellar gas to dynamical mass ratios are of order 1% in the bulge, about 1.5% in the ring followed by a rise to 3%. The bulge gas may have originated in mass loss from bulge stars; in that case, the molecular ring is probably caused by a decrease in evacuation efficiency at the bulge outer edge.

Key words: Galaxies – individual (NGC 7331) – ISM – spiral – structure; Radio lines – galaxies; ISM – molecules

1. Introduction

NGC 7331 is an isolated spiral galaxy of type Sb(rs)I-II with prominent dust lanes close to its centre (Kormendy &

Send offprint requests to: F.P. Israel

Table 1. NGC 7331 parameters

Type ^a	Sb(rs)I-II
Optical Centre:	
R.A. (1950) ^b	$22^{\text{h}}34^{\text{m}}47.7^{\text{s}}$
Decl.(1950) ^b	$34^{\circ}09'35''$
Radio Centre :	
R.A. (1950) ^c	$22^{\text{h}}34^{\text{m}}46.6^{\text{s}}$
Decl.(1950) ^c	$34^{\circ}09'21''$
V_{LSR}^d	831 km s^{-1}
Distance D^e	14.3 Mpc
Inclination i^f	74.8°
Position angle P^f	167°
Luminosity L_{B}^g	$5.0 \times 10^{10} L_{\text{B}\odot}$
Scale	$14.5''/\text{kpc}$

Notes to Table 1:

^a RSA (Sandage & Tammann 1987)

^b Dressel & Condon (1976)

^c Begeman (1987); Cowan et al. (1994)

^d Corresponding to $V_{\text{Hel}} = 820 \text{ km s}^{-1}$ (Begeman 1987)

^e Tully (1988); corresponds to $H_0 = 75 \text{ km s}^{-1}$

^f HI-derived parameters from Begeman (1987)

^g Begeman (1987) rescaled to $D = 14.3 \text{ Mpc}$

Norman 1979; Sandage & Tammann 1987). Table 1 summarizes the relevant parameters of NGC 7331. A ringlike distribution of dust surrounding the bulge was suggested by Telesco et al. (1982). Such a distribution is also apparent in radio continuum maps (Cowan et al. 1994), but only vaguely in HI maps (Bosma 1978; Begeman 1987). A strong ring signature in CO emission was claimed by Young & Scoville (1982).

Several galaxies are thought to host a molecular ring structure (see e.g. Braine et al. 1993), such as the ring in our own Galaxy discovered by Scoville & Solomon (1975) and the one in M 31 (Stark 1979; Dame et al. 1994; Koper 1993). The latter serves to illustrate a dilemma commonly facing the interpretation of CO maps, especially those of highly inclined galaxies where rings are most easily discerned: the conspicuous molecular structure may in fact consist of spiral arm segments that only in projection sug-

gest a ringlike structure. Two-dimensional CO mapping of NGC 7331 by von Linden et al. (1996) and Tosaki & Shioya (1997) support the latter interpretation. Although molecular rings have been identified in or claimed for other galaxies, the case of NGC 7331 is of interest because it resembles M 31 in being a large spiral galaxy of relatively early type, containing a prominent stellar bulge. It has also been claimed to have, as M 31, very little CO emission inside its molecular ring (Young & Scoville 1982; Tosaki & Shioya, 1997). NGC 7331 even resembles M 31 in its high inclination (75° and 77° respectively – Arp & Kormendy 1972, Sandage & Tammann 1987). Its radio structure is a stronger version of that of M 31 (Cowan et al. 1994). NGC 7331 also contains a clear, but patchy radio continuum ring. Inside the ring, little or no radio emission is found, except for a compact nuclear source. The luminosity of this source is 3–4 times that of Sgr A, and a thousand times stronger than the nucleus of M 31. It is associated with a nuclear X-ray source (Stockdale et al. 1998). Ring-like distributions of interstellar dust are also seen at mid-infrared (Smith 1998) and submillimeter (Bianchi et al. 1998) wavelengths, but they are not nearly as evident at the far-infrared wavelengths inbetween (Smith & Harvey 1996; Alton et al. 1998).

An unusual characteristic of NGC 7331 is the rather low $J=2-1/J=1-0$ CO transitional ratio of 0.5–0.7 reported by Braine et al. (1993) and von Linden et al. (1996). This is quite different from most other galaxies observed in CO, where the two transitions are usually of similar strength. However, such low transitional ratios have also been found for individual dark clouds in the central parts of M 31 (Allen & Lequeux 1993). These were interpreted as evidence for very cold ($T_{\text{kin}} < 5$ K) and tenuous ($n \approx 100 \text{ cm}^{-3}$) molecular clouds by Loinard et al. (1995), but Israel et al. (1998) showed that they are more likely caused by filamentary gas at temperatures $T_{\text{kin}} \approx 10$ K present at both low and high densities. Given the similarities between NGC 7331 and M 31, it is of interest to investigate whether such a state of affairs also applies to the central region of NGC 7331.

In this paper, we present a fully sampled map of NGC 7331 in the $J=2-1$ ^{12}CO transition over an area of $1.3'$ by $3.5'$. In addition, we have measured the first three ^{12}CO and ^{13}CO transitions as well as the 492 GHz CI transition towards the central region of the galaxy, allowing us to narrow down the permitted range of the apparently unusual physical conditions in the center.

2. Observations

Details relevant to the observations are listed in Table 2; the system temperatures given are the means for the respective runs. Observations in the $J=1-0$ transition were obtained with the IRAM 30 m telescope in service mode, at the optical and radio centre positions respectively, sepa-

Table 2. Observations Log

Transition	Date (MM/YY)	Freq (GHz)	T_{sys} (K)	Beamsize ($''$)	η_{mb}
^{12}CO					
$J=1-0$	07/97	115	350	21	0.74
$J=2-1$	11/91	230	850	21	0.63
	08-10/92		600	21	0.63
	01/96		500	21	0.69
	12/97		260	21	0.69
$J=3-2$	05/93	345	720	14	0.53
	07/95		900	14	0.58
^{13}CO					
$J=1-0$	07/97	110	200	21	0.74
$J=2-1$	09/93	220	660	21	0.63
	12/97		320	21	0.69
CI					
$^3\text{P}_1-^3\text{P}_0$	11/96	492	1900	10	0.53

rated by $\Delta\alpha = 13.7''$, $\Delta\delta = 14.0''$. The ^{13}CO observations were bracketed by the ^{12}CO observations.

All other observations were carried out with the 15m James Clerk Maxwell Telescope (JCMT) on Mauna Kea (Hawaii) ¹. Up to 1993, we used a 2048 channel AOS back-end covering a band of 500 MHz (650 km s^{-1} at 230 GHz). After that year, the DAS digital autocorrelator system was used in bands of 500 and 750 MHz. Resulting spectra were binned to resolutions of $4 - 10 \text{ km s}^{-1}$, except for the 492 GHz CI spectrum which was binned to 18 km s^{-1} on order to obtain a sufficiently high signal-to-noise ratio. Only linear baseline corrections were applied to the spectra. All spectra were scaled to a main-beam brightness temperature, $T_{\text{mb}} = T_{\text{A}}^*/\eta_{\text{mb}}$; relevant values for η_{mb} are given in Table 2. Spectra are shown in Fig. 1 and summarized in Table 3. Position A (indicated in Figure 2) is that of the radio nucleus, the actual galaxy center. Along the minor axis, the beam just fills the space between the ring components. Positions B and C are close to the minor axis at deprojected radii $R = 4.5 \text{ kpc}$ and $R = 8.2 \text{ kpc}$ respectively; position B is centered on the CO ring. Because of the pronounced tilt of the galaxy, $21''$ circular observing beams sample elongated ellipses in the plane of the galaxy, covering a range of 5.55 kpc in the minor axis direction. The beams covering positions B and C overlap (see Figure 2); positions A and B are essentially independent.

For the $J=2-1$ mapping observations, the integration time was typically 400 seconds per spectrum, on and off

¹ The James Clerk Maxwell Telescope is operated on a joint basis between the United Kingdom Particle Physics and Astrophysics Council (PPARC), the Netherlands Organisation for Scientific Research (NWO) and the National Research Council of Canada (NRC).

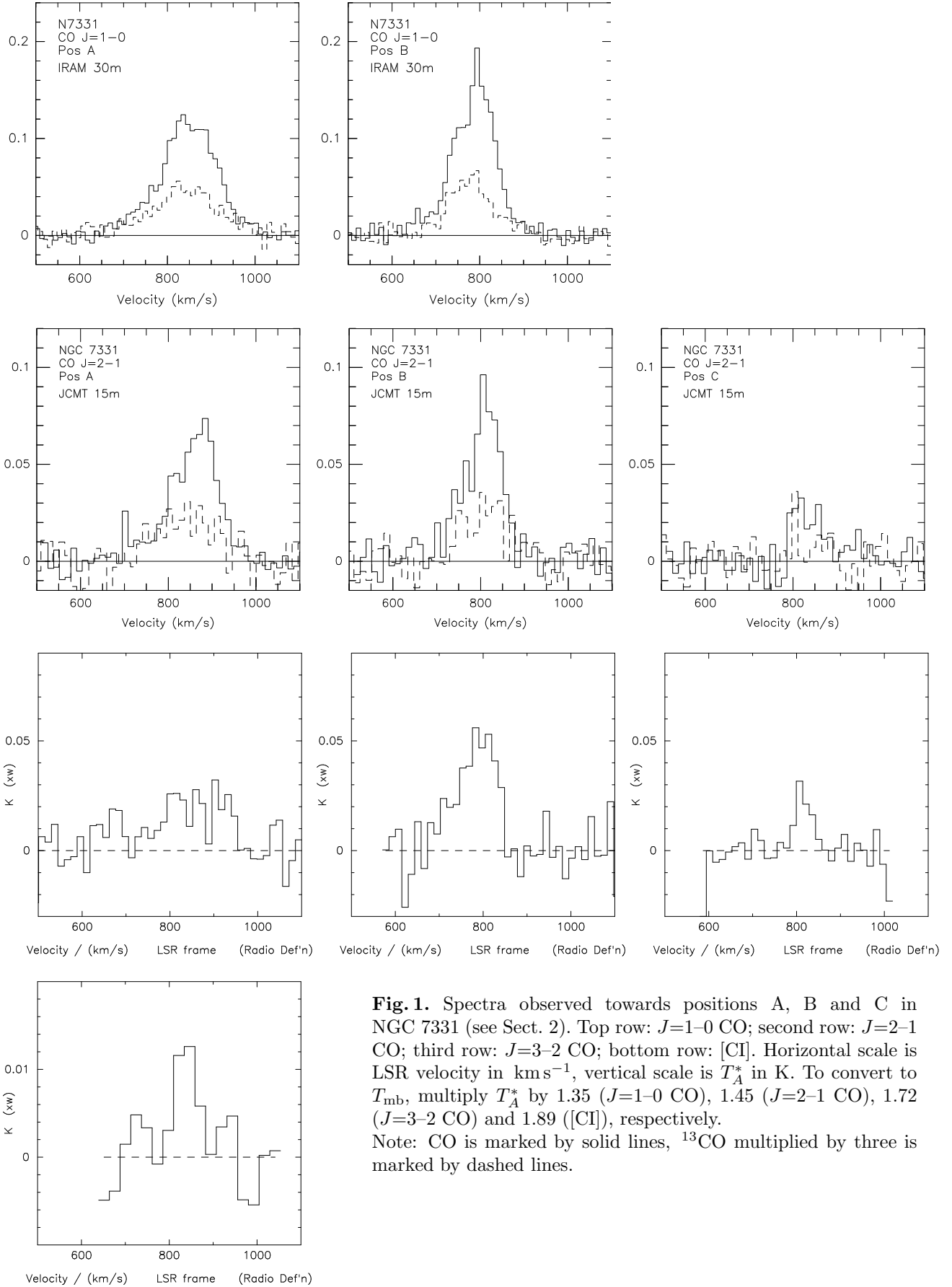


Table 3. CO and CI line intensities in NGC 7331

Transition		Resolution ($''$)	T_{mb} (mK)	$\int T_{\text{mb}} dV$ (K km s $^{-1}$)
A : $\alpha = 22:34:46.6$; $\delta = 34:09:21$				
$J=1-0$	^{12}CO	21	162	26 ± 2
	^{13}CO	21	21	3.9 ± 0.4
$J=2-1$	^{12}CO	21	100	14 ± 2
	^{13}CO	21	13	2.5 ± 0.6
$J=3-2$	^{12}CO	14	43	7.5 ± 1.3
		21	49	8.8 ± 1.5
$^3\text{P}_1-^3\text{P}_0$	CI	10	30	1.9 ± 0.3
B : $\alpha = 22:34:47.7$; $\delta = 34:09:35$				
$J=1-0$	^{12}CO	45 ^a	47	7 ± 1
	33 ^b		170	27 ± 4
	21		245	25 ± 2
	^{13}CO	21	27	3.3 ± 0.4
$J=2-1$	^{12}CO	21	109	12 ± 2
	^{13}CO	21	13	1.8 ± 0.3
$J=3-2$	^{12}CO	14	100	10 ± 2
	21 ^c		–	10 ± 4
C : $\alpha = 22:34:48.9$; $\delta = 34:09:34$				
$J=1-0$	^{12}CO	21 ^d	–	10 ± 2
$J=2-1$	^{12}CO	21	36	3.5 ± 1
	^{13}CO	21	5:	0.6 ± 0.3
$J=3-2$	^{12}CO	14	53	2.5 ± 0.5
	21 ^c		–	3.5 ± 1.5

Notes to Table 3:

- a. From Young et al. (1995); b. From Elfhag et al. (1996);
c. Extrapolated value; d. From von Linden et al. (1996)

the source. After binning to a velocity resolution of 5 km s $^{-1}$, the resulting r.m.s. noise and baseline deviations were of the order of 20 mK over most of the band.

3. Results

3.1. CO distribution

In the $J=1-0$ and $J=2-1$ transitions, the integrated intensities of both CO isotopes are rather similar for positions A and B, indicating a fairly smooth central distribution of relatively strong CO. This is consistent with the large (50%) fraction of flux found to be missing by Tosaki & Shioya (1997) in their $J=1-0$ CO interferometer map. The results presented here and by von Linden et al. (1996) are, however, inconsistent with the folded major axis profile obtained by Young & Scoville (1982) and shown in more detail by Young et al. (1995), which exhibits both a pronounced lack of CO at the centre and a strong peak at a radial distance of 45'' (3 kpc). From the data in Table

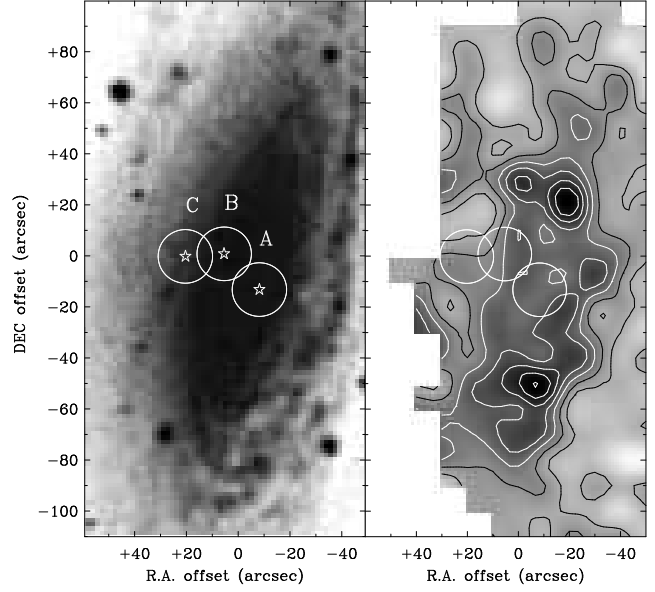


Fig. 2. Left: Digitized sky survey image of NGC 7331 with observed positions A, B and C (see Table 3) marked. Size of circle corresponds to 230 GHz beamsize. Right: Distribution of $J=2-1$ ^{12}CO emission in NGC 7331, integrated over a velocity range $V_{\text{LSR}} = 530 - 1130$ km s $^{-1}$. Contours are in steps of $\int T_{\text{mb}} dV = 4$ K km s $^{-1}$. Observed positions A, B and C are indicated by circles. Table 1.

2 and the results obtained by von Linden et al. (1996), it appears that the central integrated value given by Young et al. (1995) is too low by more than a factor of two. Thus, *there is no significant central ‘hole’ in the distribution of CO emission*, at least not on the scale of our 20'' beam.

A full-resolution contour map of the $J=2-1$ CO intensity, integrated over the velocity range of 530 to 1130 km s $^{-1}$ is shown in Fig. 2. The map shows a good overall resemblance to the $J=1-0$ CO map obtained at slightly lower resolution by von Linden et al. (1996). This is also true for the major axis position-velocity diagram (not shown here). In Fig. 2, the elliptical outline of a low-contrast ring around the center can be discerned; peaks of CO emission occur at positions 30'' north and 50'' south. The latter two more or less correspond to the radial distance of the molecular ring proposed by Young & Scoville (1982). The map covers the brightest part of the optical image also shown in Figure 2 (for better images, see panel 40 in the atlas by Sandage & Bedke 1988). In this image, a large, overexposed bulge is surrounded by dust lanes and irregular spiral arms traced by HII regions. The CO maxima at $\Delta\delta = -50''$ and $+30''$ fall on either side of the bulge, and the ring traces dusty spiral arms close to the bulge, especially on the western side. Most of the reddening of NGC 7331 occurs in this western spiral arm (Telesco et al. 1982; Bianchi et al. 1998). On the eastern side of the CO map, faint emission due to a more distant

major spiral arm is seen as well. The HI map obtained by Begeman (1987) at a very similar resolution shows an incomplete ‘ring’ of neutral hydrogen. The CO emission from the outlying spiral arm coincides with a relatively bright part of this HI ‘ring’. Most of the CO emission is, however, well inside it and coincides with the radio continuum ring mapped by Cowan et al. (1994). The main CO peaks are at the northern and southern extremities of the radio continuum ring.

In the velocity-integrated single-dish CO map (Fig. 2), the ring is only weakly visible. Its presence is more clearly revealed in the interferometer map of Tosaki & Shioya (1997) and in Fig. 3. This figure shows the distribution of $J=2-1$ ^{12}CO over the same region, but now integrated over velocity bins of 40 km s^{-1} only. Between velocities $V_{\text{LSR}} = 600$ and 1000 km s^{-1} , the maps show a double structure. The double-peak structure seen in Fig. 3 extends over most of the part of NGC 7331 characterized by rigid rotation (cf. von Linden et al. 1996). A similar pattern, with the limitations imposed by interferometric techniques, is also evident in the channel maps published by Tosaki & Shioya (1997).

3.2. Line ratios

The $^{12}\text{CO}/^{13}\text{CO}$ isotopical ratios of 6–7 are somewhat low compared to typical values around 10 found in most other external galaxies, but given the low IRAS f_{60}/f_{100} ratio of 0.3 (Rice et al. 1988) this is in line with the results obtained by Aalto et al. (1991). We find a $^{12}\text{CO } J=2-1/J=1-0$ ratio of 0.54 ± 0.10 in the center, consistent with the results obtained by Braine et al. (1993) and von Linden et al. (1996). Both $J=1-0/J=2-1$ intensities and ratio decrease away from the center. The CO transitional ratios observed in NGC 7331 are rather different from those of most other galaxies, where the lower J transitions usually have similar velocity-integrated intensities (cf. Israel & van der Werf 1996). In contrast, CO intensities in the centre of NGC 7331 decrease rapidly with increasing J level (Table 3). The $J=2-1/J=1-0$ ratios suggest subthermal excitation either at relatively low excitation temperatures or at very low column densities. However, the observed $J=3-2/J=2-1$ ratios of 0.6 or higher indicate the presence of a certain amount of warm molecular gas. Very low temperatures are also unlikely because they imply CO/ ^{13}CO ratios substantially closer to unity than is observed. We also note, in Table 4, a similarity between the ratios applicable to the D 478 cloud in the central parts of M 31 and to the emission from NGC 7331, notwithstanding the factor of 400 difference in beam surface area.

4. Analysis and discussion

4.1. Modelling of observed line intensities

We have modelled the observed intensities and their ratios by assuming the presence of two molecular gas com-

ponents of different temperature and density, a relatively cold component dominating the $J=1-0$ emission and a warmer component becoming progressively more important in the higher transitions. We have used the radiative transfer models from the Leiden astrochemistry group (Jansen 1995; Jansen et al. 1994); we included a background radiation field of $T_{\text{bg}} = 2.73 \text{ K}$. In these models kinetic temperature, molecular hydrogen density and CO respectively C column densities function as input parameters. A further constraint is provided by the chemical models discussed by Van Dishoeck & Black (1988) which show a strong dependence of the $N(\text{C})/N(\text{CO})$ column density ratio around molecular hydrogen column densities of about 10^{21} cm^{-2} . Above $N(\text{H}_2) = 2 \times 10^{21}$, virtually all carbon is in CO, whereas below $N(\text{H}_2) = 2 \times 10^{20} \text{ cm}^{-2}$ virtually all carbon is in C. The CI and CO intensities observed in position A, together with the sensitivity of the C/CO ratio to H_2 column density provide rather stringent constraints on the models acceptable for at least the center of NGC 7331.

Although the available data do not allow a precise and unique determination of the physical condition of the molecular gas in NGC 7331, they serve well to constrain the parameter space of possible solutions. For instance, cold component CO column densities cannot exceed $N(\text{CO}) \approx 10^{17} \text{ cm}^{-2}$ and warm component kinetic temperatures cannot be lower than 20 K without conflicting with observed ^{12}CO and ^{13}CO ratios. In Table 5 we list a few representative models. Note that the CO column densities listed in Table 5 are those of a single model cloud. We assume a homogeneous population of such model clouds, non-shadowing in position-velocity space, so that the actual galaxy beam-averaged column density is the sum of the model cloud column densities in the beam multiplied by their beam filling factor.

In models 4 through 7 we vary the cold component input parameters, and assume a warm component of 30 K and density $n(\text{H}_2) = 1000 \text{ cm}^{-3}$. In models 2 and 3, we have changed the warm component temperature to 40 K and 20 K, and in model 1 we assume a more complex situation. In addition to the warm component, the cold component itself is structured into a high-density and a low-density contributor. It is a scaled version of the single-temperature, dual-density model ($T_{\text{kin}} = 10 \text{ K}$; $n(\text{H}_2) = 100 \text{ cm}^{-3}$ and 3000 cm^{-3}) applied to the M 31-D 478 cloud complex by Israel et al. (1998). Although a warm component must be included, its nature is unclear. Given the large linear beamsize ($1.5 \times 5.5 \text{ kpc}$) in the plane of the galaxy, this warm component may represent discrete, starforming cloud complexes at some distance from the center. In all models, $J=1-0$ CO intensities are dominated by emission from the cold component with contributions of about 75%, 70% and 85% for positions A, B and C respectively. In contrast, the $J=3-2$ CO intensities are all dominated by emission from the warm component. For the optically thin ^{13}CO transitions the

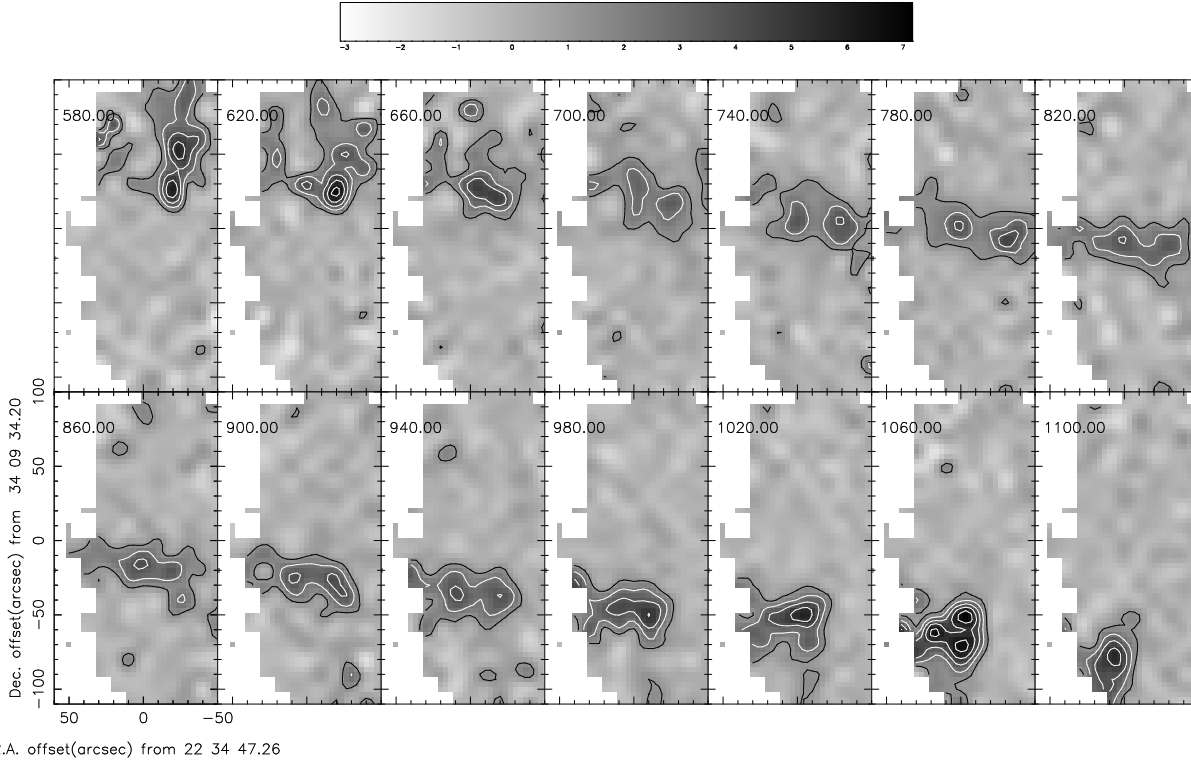


Fig. 3. $J=2-1$ ^{12}CO channel maps of NGC 7331. Emission is integrated over velocity bins of 40 km s^{-1} ; central velocities are marked in the panels. Contours are in steps of $\int T_{\text{mb}} dV = 2 \text{ K km s}^{-1}$.

Table 4. Integrated line ratios in the centre of NGC 7331

Transitions		pos. A	pos B.	pos. C	D 478 ^a
^{12}CO	(2-1)/(1-0)	0.54 ± 0.10	0.51 ± 0.10	0.35 ± 0.11	0.42 ± 0.08
	(3-2)/(2-1)	0.63 ± 0.15	0.78 ± 0.35	1.0 ± 0.41	0.33 ± 0.10
^{13}CO	(2-1)/(1-0)	0.64 ± 0.2	0.55 ± 0.1	—	0.45 ± 0.15
$^{12}\text{CO}/^{13}\text{CO}$	(1-0)	6.7 ± 1.1	7.8 ± 1.2	—	8.8 ± 1.8
	(2-1)	5.6 ± 1.6	7.2 ± 1.6	5.8 ± 3.3	8.4 ± 1.7
CI/CO(2-1)		0.21 ± 0.07	—	—	0.24 ± 0.05

Note: a. Dark cloud in M 31; see Allen et al. (1995); Loinard & Allen (1998); Israel et al. (1998).

Table 5. Model parameters for NGC 7331

Model	Cold Component			Warm Component	
	Kinetic	Gas	CO Column	Kinetic	Gas
	Temperature T_{kin} (K)	Density $n(\text{H}_2)$ (cm^{-3})	Density $N(\text{CO})/dV$ ($10^{17} \text{ cm}^{-2} (\text{K km s}^{-1})^{-1}$)	Temperature T_{kin} (K)	Density $n(\text{H}_2)$ (cm^{-3})
1	10/10 ^a	100/3000	0.7/7.0	30	3000
2	10	300	1.0	40	1000
3	10	300	1.0	30	1000
4	10	300	1.0	20	1000
5	10	100	1.0	30	1000
6	10	300	0.1	30	1000
7	10	100	0.1	30	1000

Note: ^a Cold component assumed to consist of both low and high density gas as in D 478; see Israel et al. (1998).

Table 6. CO and C in NGC 7331

Model	Predicted CI Intensity $\int T_{\text{mb}} dV$ (K kms ⁻¹)	Beam-Averaged Column Densities $N(\text{CO})$ $N(\text{C})$ $N(\text{H}_2)$ (10 ²⁰ cm ⁻²)			Conversion Factor X (10 ²⁰ cm ⁻² / K kms ⁻¹)	Mass per Beam $M(\text{H}_2)$ M_{gas} (10 ⁷ M _⊙)		Face-on Mass Density $\sigma(\text{H}_2)$ σ_{gas} (M _⊙ /pc ⁻²)	
Position A; $N_H/N_C = 1700$; $N(HI) = 5 \times 10^{20}$ cm ⁻²									
1	2	0.011	0.006	12	0.4	3	5	5	8
2	4	0.012	0.040	42	1.6	11	15	17	24
3	4	0.009	0.041	40	1.5	10	14	16	23
4	4	0.008	0.042	40	1.5	10	14	16	23
5	4	0.009	0.051	48	1.9	13	18	20	28
6	8	0.005	0.045	39	1.5	10	15	16	23
7	9	0.008	0.089	80	3.1	21	29	33	46
Position B; $N_H/N_C = 2300$; $N(HI) = 9 \times 10^{20}$ cm ⁻²									
1	2.5	0.011	0.007	16	0.6	4	7	7	12
3	4	0.006	0.030	37	1.5	10	15	15	23
Position C; $N_H/N_C = 3000$; $N(HI) = 9 \times 10^{20}$ cm ⁻²									
1	0.7	0.004	0.003	8	0.8	2	4	3	7
3	1.3	0.002	0.013	19	1.9	5	8	8	13

situation is less clearcut: if we assume an intrinsic isotopic ratio of 100, emission from the cold component contributes about 25% to the $J=1-0$ emission from positions A and B, whereas this fraction increases to about 45% if we assume an isotopic ratio of 50.

4.2. CO and C column densities

In order to relate neutral carbon and carbon monoxide column densities to that of molecular hydrogen, we have used $[\text{C}]/[\text{H}]$ gas-phase abundance ratios estimated from the $[\text{O}]/[\text{H}]$ abundance. From the data tabulated by Zaritsky et al. (1994) we determined for the central beam (position A) $12 + \log (\text{O}/\text{H}) = 9.2$, i.e. $[\text{O}]/[\text{H}] = 1.5 \times 10^{-3}$. Although high, such an oxygen abundance is normal for galaxy centers (Garnett et al. 1997; van Zee et al. 1998). Using results given by Garnett et al. (1999), notably their Figures 4 and 6, we arrive at an estimated carbon abundance $[\text{C}]/[\text{H}] = 2 \pm 1 \times 10^{-3}$. As a significant fraction of all carbon will be tied up in dust particles, and not be available in the gas-phase, we adopt a fractional correction factor $\delta_{\text{c}} = 0.33$. Neglecting contributions by e.g. ¹³CO and ionized carbon, we thus find $N_{\text{H}} = [2N(\text{H}_2) + N(\text{HI})] \approx 1700 [N(\text{CO}) + N(\text{C})]$ with a factor of two uncertainty in the numerical factor. Similarly, we find for the off-center positions B and C numerical factors of 2300 and 3000. The beam-averaged column densities in Table 6 have been obtained by scaling the model cloud column densities by the ratio of actual observed CO intensity to predicted model CO intensity.

The results of our model calculations are given in Table 6. In the table we give the predicted $[\text{CI}]$ intensity I_{CI} , which can be verified observationally, the calculated

beam-averaged column densities for both CO and C, the H_2 column densities derived from these using the $N_{\text{H}}/N_{\text{C}}$ ratios and $N(\text{HI})$ values given, as well as the implied CO to H_2 conversion factor $X = N(\text{H}_2)/I_{\text{CO}}$. The neutral carbon intensities $I(\text{CI})$ were calculated under the assumption that a significant fraction (0.6–0.7) of the total atomic carbon column density is ionized and present in the form of $[\text{CII}]$. Changes in the input CO column densities do not strongly affect the resultant C column density: a substantially higher $N(\text{CO})$, for instance, implies a lower $N(\text{C})/N(\text{CO})$ ratio, yielding a relatively unchanged $N(\text{C})$. We have also performed the calculations for a ratio of 50. Generally, the ratio of 100 provides a better fit to the ¹³CO data than the ratio of 50. As the end results for the two sets are moreover very similar, we have not included the latter in the table. The results of all models are given for position A, where we have also measured the $[\text{CI}]$ intensity in a 10'' beam. However, the models apply to measurements in the 21'' beam observed or synthesized for CO. If atomic carbon is at a minimum in the center, $[\text{CI}]$ intensities in a twice larger beam may be somewhat higher, perhaps by as much as 40%. Table 6 shows that model 1 yields a very good fit, whereas models 2 through 5 are marginally possible and models 6 and 7 are ruled out. Model 1 is not unique; various other combinations of somewhat different kinetic temperatures for both cold and warm gas and somewhat different densities, yield very similar results.

As models 6 and 7 are ruled out for position A and models 2 through 5 yield almost identical final results, we present only models 1 and 3 for positions B and C. The results for position C have relatively large uncertainties due to the weakness of its emission, and the lack of a $J=1-0$

^{13}CO measurement. The results are not greatly different from those obtained at position A. Column densities decrease, and X factors increase somewhat with radius. At $T_{\text{kin}} = 10$ K, the $^3\text{P}_2\text{--}^3\text{P}_1$ [CI] transition at 809 GHz has negligible intensity, but this becomes comparable to the $^3\text{P}_1\text{--}^3\text{P}_0$ 492 GHz transition at $T_{\text{kin}} = 30$ K. The presence of the warm component can therefore be verified by future observations of the 809 GHz [CI] transition, for which we predict an intensity of 15–30% of the 492 GHz intensity. For the [CII] emission we expect intensities of the order of 5×10^{-6} erg s $^{-1}$ cm $^{-2}$ sr $^{-1}$.

Beam-averaged neutral carbon to carbon monoxide column density ratios are $N(\text{C})/N(\text{CO}) = 0.65 \pm 0.1$ and $N(\text{C})/N(\text{CO}) = 5.5 \pm 1.0$ for models 1 and 3 respectively. The former is close to the typical values 0.2–0.5 found for M 82, NGC 253 and M 83 (White et al. 1994; Israel et al. 1995; Stutzki et al. 1997; Petitpas & Wilson 1998), but the latter is much higher and is only matched by the corresponding ratio of 3–6 found in Galactic translucent clouds (Stark & van Dishoeck 1994).

4.3. Molecular hydrogen and the $I(\text{CO})$ to $N(\text{H}_2)$ ratio

Although any explanation of the observed CO intensities requires the presence of both cold and smaller amounts of warm molecular gas in NGC 7331, the range of admissible parameters is not fully constrained. The [CI] intensity observed towards the center of the galaxy, however, strongly suggests a complex physical environment of the sort represented by model 1. This model is characterized by cold molecular gas (typical temperature $T_{\text{kin}} = 10$ K) present at both high and low volume densities (typically of order a few hundred and a few thousand per cc respectively), in addition to a warmer component (temperature $T_{\text{kin}} \geq 20$ K) of high density. This is probably a simplification: in reality a range of densities and temperatures is likely to be present. As the large linear beamsize (1.5 kpc along the major axis, 5.5 kpc along the minor axis) only provides results averaged over a large radial range, the spatial distributions of the cold and the warm gas within the beam may well be different. Both kinetic temperature and mean molecular gas density in the centre of NGC 7331 are typically an order of magnitude below the values found in later-type starburst galaxies such as NGC 253 and M 82 (Israel et al. 1995; Wall et al. 1991).

Our models suggest that a large fraction of the CO emission originates from cold gas of low column density. A smaller fraction originates in much denser gas, partly at higher temperatures. The cold gas in the center of NGC 7331 appears to be similar to that in cloud complexes such as D 478 in M 31 dark and the Taurus-Auriga complex in the Milky Way; most likely, it is highly fragmented and filamentary (Israel et al. 1998). The warm gas may be heated by the nucleus and by luminous stars in the inner spiral arms and the ‘molecular ring’. The presence of energetic photons in the inner part of NGC 7331

is betrayed by $\text{H}\alpha$ + [NII] emission (see Fig. 5 by Smith & Harvey 1996) and more directly by significant UV emission (Wesselius et al. 1982) unlikely to be dominated by the spiral arms because of their high dust content (Bianchi et al. 1998).

The evaluation of the models in Tables 5 and 6 assumes a radiation field $I_{\text{UV}} \approx 1$, corresponding to $I_{1000} = 4.5 \times 10^{-8}$ photons s $^{-1}$ cm $^{-2}$ which is consistent with the longer-wavelength UV data by Wesselius et al. (1982). Such a low radiation field density is also indicated by the strength of the 7.7 and 11.3 μm dust emission features (Smith 1998). The beam-averaged column densities in Table 6 are relatively insensitive to changes in the assumed I_{UV} , because in the cold diffuse gas, most carbon is already in C rather than in CO, whereas the much smaller filling factor of the dense gas greatly reduces the effect of changes in the $N(\text{C})/N(\text{CO})$ ratio on the beam-averaged neutral carbon column density. Moreover, we expect only limited variation (by a factor of 2–3) in the radiation field density over at least the inner 5 kpc because of the smooth distribution of $\text{H}\alpha$ emission as well as the far-infrared emission between 50 μm and 200 μm (Smith & Harvey 1996; Alton et al. 1998). The quiescence of the spiral arms is illustrated by the strong excess of 450 and 850 μm emission from cold dust (Bianchi et al. 1998). Thus, the spiral arms contain a relatively large amount of cold dust especially in comparison with the central region. We are therefore confident of the derived $N(\text{H}_2)$ values in Table 6.

As C and O abundances in NGC 7331 are 2–5 times higher than those in the Solar Neighbourhood, and radiation fields are not particularly intense, we expect CO in NGC 7331 to be relatively well-shielded, so that the CO to H_2 conversion factor X should be lower than that in the Solar Neighbourhood, i.e. fewer H_2 molecules per unit CO intensity. Indeed we find values of X lower than the value of 2×10^{20} cm $^{-2}$ /K kms $^{-1}$ assumed for the Milky Way, which can also be compared to the relationship between X , radiation field intensity and metallicity found by Israel (1997). For positions A, B and C we take $[\text{O}]/[\text{H}]$ abundance ratios of 1.5, 1.3 and 1.1 in units of 10^{-3} respectively (Zaritzky et al. 1994). From high-resolution far-infrared surface brightnesses (Smith & Harvey 1996), HI column densities (Begeman (1987) and eqn. (3b) from Israel (1997), we predict values $X = 0.8, 0.7$ and 1.0 in units of 10^{20} cm $^{-2}$ /(K kms $^{-1}$) $^{-1}$ for positions A, B and C respectively. These are very close to the results from the preferred model 1, and a factor of two or more below the results for the other models. Neglect of the radiation field term in Israel’s (1997) eqn. (3b), i.e. use of his eqn. (4) predicts in the same units $X = 0.15, 0.25$ and 0.4 for positions A, B and C, i.e. much lower than any of the model results. We conclude that the low values of X in the preferred model 1 are in good agreement with both the high abundances in NGC 7331 and the relationship between X , radiation field intensity and metallicity found by Israel (1997).

With respect to the value of X derived for position A it should be noted that the large linear beamsize includes both the center of NGC 7331 and more outlying regions along the minor axis. If the latter were to be characterized by an X value closer to that of position B, the actual central X value would be significantly lower. For instance, if we assign $X = 0.6 \times 10^{20} \text{ cm}^{-2} / \text{K kms}^{-1}$ to the outer half of the CO emission, the inner half would have $X = 0.2 \times 10^{20} \text{ cm}^{-2} / \text{K kms}^{-1}$, an order of magnitude less than the Milky Way value, and well below what is suggested by the high metallicity. Such a very low value would, however, not be unexpected. For the Milky Way centre, Sodroski et al. (1995) conclude to an X -factor 3 – 10 times smaller than the ‘standard’ Galactic value. The COBE Galactic Centre data presented by Bennett et al. (1994) imply lower CO transition ratios somewhat similar to those in NGC 7331.

Another way of verifying the derived H_2 column densities is provided by the submillimeter observations presented by Bianchi et al. (1998). For $F_{850\mu\text{m}} = 50 \text{ mJy}$ and $T = 20 \pm 3 \text{ K}$ in a $30'' \times 40''$ beam (Bianchi et al. 1998), we derive a beam-averaged $A_V = 6.6$ (-1.2, +2.2). Furthermore assuming that the dust to gas ratio is proportional to metallicity, we modify the Galactic relation between total hydrogen column density and visual extinction (Bohlin et al. 1978) to $N_{\text{H}} = 0.6 \times 10^{21} A_V \text{ cm}^{-2}$. This implies a column density $N(\text{H}_2) = 2(-0.4, +0.6) \times 10^{21} \text{ cm}^{-2}$ (corresponding to $X = 0.75(-0.15, +0.25) \times 10^{20}$). The similarly obtained result for position B is slightly lower. These results are thus in rather good agreement, given the various uncertainties, with $N(\text{H}_2) = 1.2 - 1.6 \times 10^{21} \text{ cm}^{-2}$ and $X = 0.4 - 0.6 \times 10^{20}$ found for positions A and B using model 1.

Comparison of the models and the observations allows us to draw some general conclusions on the distribution of molecular hydrogen in NGC 7331. In model 1, relative amounts of cold/tenuous, cold/dense and warm/dense molecular hydrogen gas are 45%, 30% and 25% for positions A and B. The results for position C seem to indicate a somewhat higher contribution by warm molecular gas. Using the beam-averaged H_2 column densities and the model H_2 volume densities, we find that the *average* line of sight within the beam contains cold/tenuous H_2 over about 2 pc (Model 1, positions A and B) to 0.7 pc (Model 1, position C). Both the cold and the warm dense component have *average* line-of-sight extents a factor of 50 lower. However, the observed CO temperatures are much lower than the model excitation temperatures, indicating small beam-filling factors for the molecular material. Assuming individual lines of sight within the beam to be either empty, or homogeneously filled with molecular gas, we find for those line of sights that do contain molecular gas extents of about 20 pc (cold tenuous gas), 2.5 pc (cold dense gas) and 25 pc (warm dense gas); these numbers are indicative of the maximum source size that can be expected.

Application of model 3 yields somewhat different results. Here, most of the molecular gas is in the cold/tenuous form rather than in the warm/dense phase: only 17% warm gas is required at position A, and about 5% at positions B and C. *Average* line of sight extents are 3.5 pc for cold gas at positions A and B, and half that at position C. After correction for beam filling, we find lines of sight extents of typically 115 pc for the cold molecular gas and 15% or less of that for warm gas. Only at position C a more uncertain extent of 20 pc is obtained.

The derived line of sight extents are much smaller than the length of the line of sight traversing the galaxy, which is about four times its thickness. Although the latter is not known, this length can be estimated at well in excess of a kiloparsec. Thus, only a small fraction of the volume sampled by the beam at each of the analyzed positions is filled with molecular material. This material is highly clumped or distributed in filamentary form.

4.4. Radial distribution of molecular gas

In the case of highly-inclined ring structures, major-axis position-velocity diagrams may give a misleading impression of the actual radial distribution of emitting material, because at the tangential points substantially longer lines of sight contribute to the emission. To determine the actual distribution of CO as a function of radial distance from the centre spectra, we have fitted an inclined axisymmetric disk model to the data in the velocity-integrated map (Fig. 3) by applying the Richardson-Lucy iterative scheme (Lucy 1974). In principle, with *a priori* knowledge of the (CO) velocity field, this technique can also be used to obtain radial distributions with a spatial resolution *higher* than that of the observing beam (Scoville, Young & Lucy 1983). Fig. 4 shows the fitted radial distribution of the velocity-integrated $J=2-1$ CO emission.

The fitted profile corresponds to the *face-on* radial distribution of $I'(\text{CO})_0 = \int (T_{\text{a}}^*(\text{CO}) dV)_0$. The CO luminosity starts at $I'(\text{CO})_0 = 4 \text{ K kms}^{-1}$ in the center, reaches a minimum at $R \approx 1.75 \text{ kpc}$, and reaches a maximum at $R \approx 3.5 \text{ kpc}$ after which it drops smoothly to $I'_{\text{CO}} = 2 \text{ K kms}^{-1}$. The ring-to-disk intensity contrast ratio is about 0.6. The molecular ‘ring’ is clearly discernible, but it does not dominate the CO distribution in the galaxy. Both the major-axis CO distribution and the fitted radial CO profile are different from those of M 31, where most of the CO is found farther out in the spiral arm ‘ring’ at $R=9 \text{ kpc}$, and very little CO occurs at the centre (Dame et al. 1994).

In order to determine the radial distribution of interstellar gas in NGC 7331, we have converted the CO radial profile to a radial distribution of H_2 mass densities, using the $J=1-0/J=2-1$ CO ratios and X values from Tables 4 and 6, and combined these with the radial HI profile published by Begeman (1987). Both the radial H_2 and HI profiles are also shown in Figure 4. In the inner 4.5

kpc, the H_2 mass dominates that of HI by about 40%. Beyond this, HI becomes increasingly dominant. The radial distribution of molecular gas reaches its peak (at $R = 3.1$ kpc) well before that of HI (at $R \approx 10$ kpc). Although the radial $J=2-1$ CO profile exhibits a relatively low contrast between the ring feature and the underlying disk emission, the radially increasing transitional ratios and X -values serve to enhance the contrast in H_2 . The central region is not empty, but the H_2 mass density inside the ring is only 75% of that in the ring; due to the lack of HI in the center, the relative mass density of all hydrogen is even lower with 55% of the ring value. The face-on H_2 mass distribution increases from $\sigma_{\text{H}_2} = 6 \text{ M}_\odot \text{ pc}^{-2}$ at $R = 3.1$ kpc. The total hydrogen radial mass-density distribution increases from a central value $\sigma_{\text{HI}+\text{H}_2} = 8 \text{ M}_\odot \text{ pc}^{-2}$ to $\sigma_{\text{HI}+\text{H}_2} = 14 \text{ M}_\odot \text{ pc}^{-2}$ at $R = 3.5$ kpc and then drops slowly. The gaseous fraction (including helium) of the total mass was estimated from the rotation curves given by Rubin et al. (1965) and Begeman (1987), assuming a spherical bulge and circular velocities. Inside the ring, the gas-to-total mass ratio $M_{\text{gas}}/M_{\text{dyn}}$ is about 1%. In the ring, it rises to 1.5%, and then slowly climbs to 3%. From Begeman's (1987) data, neglecting H_2 , we find in comparison a *global* ratio $M_{\text{gas}}/M_{\text{dyn}}$ of 3.2%. Even with the dominant contribution by H_2 , the gas in the inner part of NGC 7331 is only a minute fraction of the total mass.

Finally, it is of interest to compare the radial gas distributions to the radial far-infrared profiles representing interstellar dust. The $100\mu\text{m}$ far-infrared profile (Smith & Harvey 1996) is rather flat in the center, reaching a very minor maximum at about 2 kpc, after which a steep decline sets in. The $450\mu\text{m}$ and $850\mu\text{m}$ profiles show radially increasing intensities that reach a peak at about 3 kpc, the $850\mu\text{m}$ profile peaking a little farther out than the $450\mu\text{m}$ profile (Bianchi et al. 1998). The H_2 mass-density peaks at $R = 3.1$ kpc, just about coincident with the $850\mu\text{m}$ maximum. At the location of the molecular 'ring' peak, $100\mu\text{m}$ intensities are about 80% of those in the center. However, the total gas mass-density peaks slightly farther out at $R = 3.8$ kpc. Thus, emission from warm dust peaks well inside the molecular ring, and both molecular gas and cold dust peak inside the radius of highest gas mass-density. Beyond the ring peak, the decline of the $450\mu\text{m}$ and $850\mu\text{m}$ emission more or less follows that of the H_2 mass density profile. We conclude that the interstellar dust is hottest in the central region, where gas mass-densities are lowest. The mean dust temperature defined by the far-infrared ratios smoothly decreases from the center reaching a shallow minimum at about $R = 3$ kpc, i.e. at the H_2 peak, beyond which it appears to increase slightly.

4.5. Origin of bulge molecular gas and the ring

Various mechanisms for the occurrence of ring morphologies have been suggested in the literature. Interaction be-

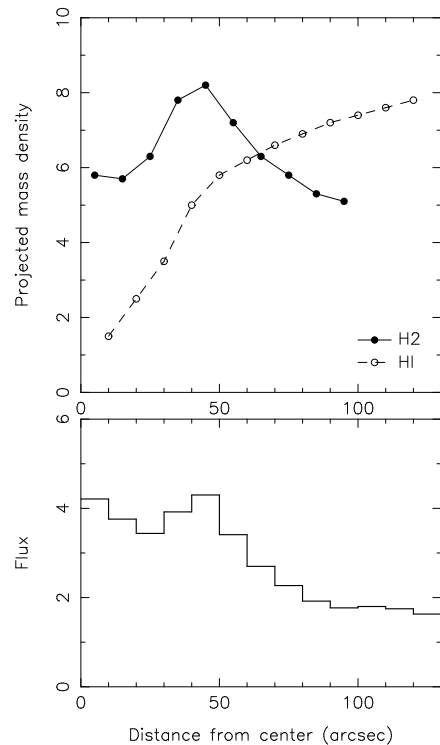


Fig. 4. Deprojected radial profiles. Bottom: Face-on radial distribution of CO emission obtained with the Richardson-Lucy scheme (see section 4.4). Vertical axis is $\int T_{\text{mb}} dV$ as would be observed perpendicular to the galaxy plane. Top: Face-on mass-densities of H_2 and HI, in units of $\text{M}_\odot \text{ pc}^{-2}$. HI data were taken from Begeman (1987).

tween magnetic fields and the gas distribution were proposed and tested by Battaner et al. (1988). Inner Lindblad resonances may be responsible (Kormendy & Norman 1979), and a ringlike feature may also result from evacuation of gas from the central regions by stellar winds (cf. Faber & Gallagher 1976; Soifer et al. 1986, Muñoz-Tuñón & Beckman 1988). Finally, as Young & Scoville (1982) suggested for NGC 7331, a ringlike appearance may also be caused by the nuclear bulge having used up the originally present molecular gas in the center.

In NGC 7331, the solid-body rotation curve rises rapidly out to $R = 3.5$ kpc after which it flattens and reaches a broad maximum at $R = 6$ kpc (see also von Linden et al. 1996). The ring is thus located just at the radius where rigid rotation is lost, but well within the radius of maximum rotational velocity ($R_{\text{ring}} = 0.6 R_{\text{Vmax}}$). This is unlike M 31, where the molecular ring is found at a radius *twice* that of peak rotational velocity (Brinks & Burton 1984; Dame et al. 1993). Both the molecular ring and the boundary of the solid-body rotation region are also just at the radius at which the light of the disk becomes dominant over that of the bulge (cf. Begeman 1987). Although the radius of the mostly nonthermal radio continuum ring radius is more difficult to determine because of its inhomogeneous

geneous structure, it appears to coincide more or less with the molecular ring, also well inside the radius of maximum rotational velocity (Cowan et al. 1994).

On the same reasoning as used by Young & Scoville (1982), we may rule out the presence of an inner Lindblad resonance in NGC 7331 as an explanation for the observed molecular ring structure, because an ILR can only occur well outside the region of solid-body rotation (e.g. Kormendy & Norman 1979). Our observations clearly show that there is no pronounced CO hole in the centre of NGC 7331, although *the derived distributions of both H₂ and total interstellar gas do show a significant central depression*. von Linden et al. (1996) have suggested that the ringlike distribution in NGC 7331 is caused by the dynamical action of a weak central bar. However, their simulations yield both a ring more massive than observed, and center more devoid of gas than observed, casting doubts on the proposed central bar.

In the case of M 31, Soifer et al. (1986) suggest that the amount of interstellar matter observed in the center of M 31 could have accumulated from late-type stellar mass loss in the bulge, and is kept low by continuous gas removal by supernova explosions and star formation. Could this also be the case in NGC 7331? It has been suggested by Prada et al. (1996) that the bulge of NGC 7331 is counter-rotating. Since the bulge gas is rotating in the normal sense, this would seem to preclude a stellar origin for the gas. However, spectroscopy by Mediavilla et al. (1997) and Bottema (1999) does not confirm the suggested counter-rotation. The total mass of the interstellar gas inside $R = 2$ kpc is $1.6 \times 10^8 M_{\odot}$. According to the reasoning outlined by Soifer et al. (1986), stellar mass loss in the bulge would accumulate this amount in 4×10^8 years. Removal of the same amount of material from the bulge requires the energy output of $6/n \times 10^5$ Type I supernovae, n being the fraction of energy available for the acceleration of interstellar material. For a Type I SN rate of $4 \times 10^{-13} L_B \text{ yr}^{-1}$ (Lang, 1992) the timescale for removal is $6.5/n \times 10^7$ years. Only if the fraction of supernova energy actually available for removal exceeds 17%, will the interstellar gas be evacuated from the bulge faster than bulge stars can manufacture it. More generally, with the assumptions from Soifer et al. (1986), the ratio of evacuation to deposition timescales is $t_e/t_d = 3.75 \times 10^{-6} v_c^2/n$. The tabulation of NGC 7331 rotation velocities by Bege-man (1987) then suggests relatively efficient evacuation in the inner 1 kpc ($t_e/t_d = 0.01/n - 0.05/n$), and much less efficient evacuation at the edge of the bulge ($R = 4$ kpc; $t_e/t_d = 0.24/n$). The radial decrease of the ratio of far-infrared emission to H₂ mass-density found above may be related to this finding. It thus appears that the relatively small amounts of interstellar gas in the bulge of NGC 7331 ($M_{\text{gas}}/M_{\text{dyn}} \approx 0.01$) also may well be the result of mass loss from the bulge stars themselves, rather than the result from a net inflow of molecular material from greater radii.

5. Conclusions

1. Analysis of the $J=2-1$ ¹²CO distribution and kinematics shows the presence of enhanced molecular emission in a ringlike zone in NGC 7331, peaking at a radial distance of 3.5 kpc with a width of about 2 kpc. At $R = 3.5$ kpc, the velocity-integrated CO intensity of the ring itself is about 0.6 times that of the underlying more smoothly distributed CO emission that fills the entire bulge of NGC 7331.
2. The velocity-integrated CO intensities in the center of NGC 7331 decrease strongly with increasing rotational level. The intensities in the $J=1-0$, $J=2-1$, $J=3-2$ transitions are in the ratio of 1.0 : 0.55 : 0.35 respectively. The observed ¹²CO/¹³CO isotopic ratios are 6.7 and 5.6 in the $J=1-0$ and $J=2-1$ transitions respectively. Positions at larger radial distances have similar ratios, albeit with somewhat stronger $J=3-2$ CO emission, and weaker ¹³CO emission. Weak [CI] emission was detected from the center.
3. Modelling of the observed line ratios suggest a multi-component molecular medium. Gas with a kinetic temperature of about 10 K appears to be present at both low and high densities. At high densities, a warmer component with a kinetic temperature of 20 K or more is also present within the observing beams. The gas is probably distributed in a clumpy and filamentary form.
4. Assuming a [C]/[H] abundance ratio of the order of $1-2 \times 10^{-3}$, the mean CO-to-H₂ conversion factor is $X_{\text{N7331}} = 4 \times 10^{19} \text{ cm}^{-2}$ in the bulge region, and double that value in the ring and beyond. These values are well below those found in the Solar Neighbourhood, but they are consistent with the high metallicity of NGC 7331 and with submillimeter dust observations.
5. In the bulge, interstellar gas (HI + H₂ + He) mass densities, projected onto the plane of the galaxy, are of the order of $11 M_{\odot} \text{ cm}^{-2}$. In the ring itself, now properly placed at $R = 3.1$ kpc, the gas mass density is almost twice as high. Within the ring, the interstellar gas mass is dominated by the molecular hydrogen contribution. Gas to total (dynamical) mass ratios are about 1 % in the center and about 1.5 % in the ring.
6. The molecular ring coincides more or less with the mostly nonthermal radio continuum ring and the 850 μm ring representing emission from cold dust. Emission from warmer dust in the 100 μm wavelength range peaks well inside the molecular ring; dust temperatures appear to be decreasing with radius reaching a minimum in the ring. The radial distribution of HI reaches its maximum well beyond the molecular ring.
7. The molecular ring is well inside the radius of peak rotational velocity. Its maximum is just at the edge of the region of solid-body rotation, and just at the radius where disk light becomes dominant over bulge light. The ring is not associated with an inner Lind-

blad resonance. The molecular gas inside the ring may have originated from mass loss by late type stars in the bulge. If this is the case, the ring is probably the result of wind-driven gas removal from the center.

Acknowledgements. We are indebted to Ewine van Dishoeck and David Jansen for providing us with their detailed radiative transfer models. We also thank the JCMT personnel, in particular Remo Tilanus, for their support and help in obtaining the observations discussed in this paper, and Jeroen Stil for considerable help in producing Figure 2. The IRAM observations were kindly obtained for us by Gabriel Paubert in service mode.

References

- Aalto S., Black J.H., Johansson L.E.B., Booth R.S., 1991, *A&A* 249, 323
- Allen R.J., Lequeux J., 1993, *ApJL* 410, L15
- Allen R.J., Le Bourlot J., Lequeux J., Pineau des Forêts G., Roueff E., 1995, *ApJ* 444, 157
- Alton P.B., Trewella M., Davies, J.I. et al., 1998, *A&A* 335, 807
- Arp H.C., Kormendy J., 1972, *ApJL* 178, L101
- Battaner E., Florido E., Sanchez-Saavedra M.L., 1988, *ApJ* 331, 116
- Begeman K., 1987, Ph.D. Thesis, University of Groningen (NL)
- Bennett C.L., Fixsen D.J., Hinshaw G., et al. 1994, *ApJ* 434, 587
- Bianchi S., Alton P.B., Davies J.I., Trewella M. 1998, *MNRAS* 298, L49
- Bohlin R.C., Savage B.D., Drake J.F., 1978, *ApJ* 224, 132
- Bosma A.: 1978, Ph.D. thesis, University of Groningen (NL)
- Bottema R.: 1999, *A&A* 348, 77
- Braine, J., Combes F., Casoli F., et al., 1993, *ApJS* 97, 887
- Brinks E., Burton W.B., 1984, *A&A* 141, 195
- Cowan J.J., Romanishin W., Branch D., 1994, *ApJL* 436, L139
- Dame T.M., Koper E., Israel F.P., Thaddeus P., 1994, *ApJ* 418, 730
- Dressell L.L., Condon J.J. 1976, *ApJS* 31, 187
- Elfhag T., Booth R.S., Höglund B., Johansson L.E.B., Sandquist Aa., 1996, *A&AS* 115, 439
- Faber S.M., Gallagher J.S., 1976, *ApJ* 204, 365
- Garnett D.R., Shields G.A., Skillman E.D., Sagan S.P., Dufour R.J., 1997, *ApJ* 489, 63
- Garnett D.R., Shields G.A., Peimbert M., et al. 1999 *ApJ* 513, 168
- Israel F.P., 1997, *A&A* 328, 471
- Israel F.P., White G.J., Baas F., 1995, *A&A* 302, 343
- Israel F.P., van der Werf P.P., 1996, in: *Cold Gas at High Redshift*, ed. M.N. Bremer, P.P. van der Werf, H.J.A. Röttgering, C.L. Carilli (Dordrecht: Kluwer), p. 429
- Israel F.P., Tilanus R.P.J., Baas F., 1998, *A&A* 339, 398
- Jansen D.J., 1995, Ph.D. thesis, University of Leiden (NL)
- Jansen D.J., van Dishoeck E.F., Black J.H., 1994, *A&A* , 282, 605
- Koper E. 1993, Ph.D. thesis, University of Leiden (NL)
- Kormendy J., Norman C.A., 1979, *ApJ* 233, 539
- Lang K.R., 1992, *Astrophysical Data*, (New York: Springer), p. 703
- Loinard L., Allen R.J., Lequeux J., 1995, *A&A* 301, 68
- Loinard L., Allen R.J., 1998, *ApJL* 499, 277
- Lucy L.B., 1974, *ApJ* 79, 745
- Mediavilla E., Arribas S., García-Lorenzo B., del Burgo C., 1997, *ApJ* 488, 682
- Muñoz-Tuñón C., Beckman J.E., 1988, *Ap&SS*, 147, 173
- Petitpas G.R., Wilson C.D., 1998, *ApJ* 503, 219
- Prada F., Gutiérrez C.M., Peletier R.F., McKeith C.D., 1996, *ApJL* 463, L9
- Rice W., Lonsdale C.J., Soifer B.T., et al., 1988, *ApJS* 68, 91
- Rubin V.C., Burbidge E.M., Burbidge G.R., Crampin D.J., 1965, *ApJ* 141, 759
- Sandage A., Tammann G.A., 1987, *A Revised Shapley-Ames Catalog of Bright Galaxies*, second edition, Carnegie Institution of Washington Publication 635 (Washington, D.C.: Carnegie Institution of Washington).
- Sandage A., Bedke J., 1988, *Atlas of Galaxies*, NASA-SP 496 (Washington, D.C.: NASA).
- Scoville N.Z., Solomon P.M., 1975, *ApJL* 199, L105
- Scoville N.Z., Young J.S., Lucy L.B., 1983, *ApJ* 270, 443
- Smith B.J., 1998, *ApJ* 500, 181
- Smith B.J., Harvey P.M., 1996, *ApJ* 468, 139
- Sodroski T.J., Odegard N., Dwek E., et al., 1995, *ApJ* 452, 262
- Soifer B.T., Rice W.L., Mould J.R., et al., 1986, *ApJ* 304, 651
- Stark A.A. 1979, Ph.D. thesis, Princeton University (USA)
- Stark R., van Dishoeck E.F., 1994, *A&A* 286, 443
- Stockdale C.J., Romanishin W., Cowan J.J., 1998 *ApJ* 508, 33
- Stutzki J., Graf U.U., Honingh C.E., et al. 1997, *ApJL* 477, 33
- Telesco C.M., Gatley I., Steward J.M., 1982, *ApJ* 263, L13
- Tosaki T., Shioya Y., 1997, *ApJ* 484, 664
- Tully R.B., 1988, *Nearby Galaxies Catalog*, (Cambridge: Cambridge University Press)
- van Dishoeck E.F., Black J.H., 1988, *ApJ* 334, 771
- van Zee L., Salzer J.J., Haynes M.P., O'Donoghue A.A., Balonek T.J., 1998 *AJ* 116, 280
- von Linden S., Reuter H.-P., Heidt J., Wielebinski R., Pohl M., 1996, *A&A* 315, 52
- Wall W.F., Jaffe D.T., Israel F.P., Bash F.N., 1991, *ApJ* 380, 384
- Wesselius P.R., van Duinen R.J., de Jonge A.W., et al., 1982, *A&AS* 49, 427
- White G.J., Ellison B., Claude S., Dent W.R.F., Matheson D.N., 1994, *A&A* 284, L23
- Young J.S., Scoville, N.Z., 1982, *ApJL* 260, L41
- Young J.S., Xie S., Tacconi L., et al. 1995, *ApJS* 98, 219
- Zaritsky D., Kennicutt R.C., Huchra J.P., 1994, *ApJ* 420, 87